NANO LETTERS

Letter

pubs.acs.org/NanoLett

Strain and Orientation Modulated Bandgaps and Effective Masses of Phosphorene Nanoribbons

Xiaoyu Han, Henry Morgan Stewart, Stephen A. Shevlin, C. Richard A. Catlow, and Zheng Xiao Guo*

Department of Chemistry, University College London, London WC1E 6BT, United Kingdom

Supporting Information

ABSTRACT: Passivated phosphorene nanoribbons, armchair (a-PNR), diagonal (d-PNR), and zigzag (z-PNR), were investigated using density functional theory. Z-PNRs demonstrate the greatest quantum size effect, tuning the bandgap from 1.4 to 2.6 eV when the width is reduced from 26 to 6 Å. Strain effectively tunes charge carrier transport, leading to a sudden increase in electron effective mass at +8% strain for a-PNRs or hole effective mass at +3% strain for z-PNRs, differentiating the (m_h^*/m_e^*) ratio by an order of magnitude in each case. Straining of d-PNRs results in a direct to indirect band gap transition at either −7% or +5% strain and therein creates degenerate energy valleys with potential applications for valleytronics and/or photocatalysis.

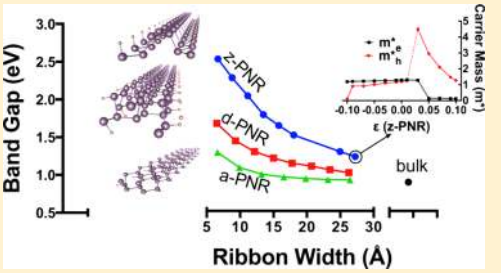

KEYWORDS: *Phosphorene, black phosphorus, nanostructures, band structure, strain effect*

One of the most critical and challenging issues facing the electronics industry is the development of alternatives to silicon-based materials so as to enable large improvement in device performance.[1−3] Considerable efforts have been devoted to 2D materials, such as graphene,[4] which despite promising charge transport properties is unable to function as a switch in transistor devices due to the lack of an intrinsic bandgap. To ameliorate this problem, several avenues of research have been pursued, including functionalization,[5] nanostructuring,[6−9] and substrate engineering.[10,11] Results to date are inconclusive and so alternative materials are sought.

The recent exfoliation of black phosphorus,[12,13] which consists of weakly stacked layers of a quasi-planar corrugated half-honeycomb structure, dubbed phosphorene, has garnered huge experimental and theoretical interest due to its relatively large and direct bandgap and good charge carrier mobilities,[14−18] Presently, several open questions remain: is it possible to synthesize this material at industrial scales? What is the nature of the strongly anisotropic conducting behavior, for example, the drain current is strongly angular dependent.[12] And what are the effects of nanostructuring on the electronic and optical properties of this material?

To resolve this last question and taking inspiration from recent experimental work on the ballistic transportation of graphene nanoribbons,[19] we have investigated the structural and electronic properties of phosphorene nanoribbons (PNRs).[20,21] Realistic stable nanoribbons were considered, for example, any bonds that are cleaved are passivated with hydrogen. To our knowledge there are two other recent publications on PNRs.[21,22] The former only considers nanoribbons with no passivating atoms that are not comparable to our system, and the latter only considers a-PNR and z-PNR structures without strain. We show that out of the three lowest energy cleavage directions, one in particular demonstrates strong quantum size effects that increase the magnitude of the bandgap, and we show that this effect is related to the spatial extent of the valence band edge (VBE) and conduction band edge (CBE) states. The effects of strain on the transport properties of phosphorene were theoretically investigated by calculation of the hole and electron effective masses at the VBE and CBE, respectively. We identify that the charge transport properties, based on the analysis of the effective mass, can be modified by uniaxial straining of the nanoribbons, analogous to the findings for biaxial straining on phosphorene.[23] We demonstrate that both the size of the bandgap and the transport properties (e.g., electron and hole transport) of the PNRs can be extensively modified by (uniaxial) straining, allowing the tuning of the material for several applications, such as solid-state lighting, light-emitting diodes, and flat panel displays. Furthermore, our findings indicate that it is possible to tune the directness of the bandgap by uniaxial straining of a particular nanoribbon structure, and that the resulting direct and indirect bandgaps are degenerate at a given strain, potentially allowing segregation of electrons and/or holes of the same energy by momentum and for valley effects to manifest.

We have performed plane-wave electronic structure calculations within the density functional theory (DFT) using projected augmented wave (PAW) potentials to treat the core electrons. All calculations were performed using the Vienna ab initio Simulation Package (VASP).[24,25] Unless explicitly stated otherwise, we present results using crystal lattices, geometries,

Received: May 3, 2014
Revised: June 27, 2014

dx.doi.org/10.1021/nl501658d | *Nano Lett.* XXXX, XXX, XXX−XXX

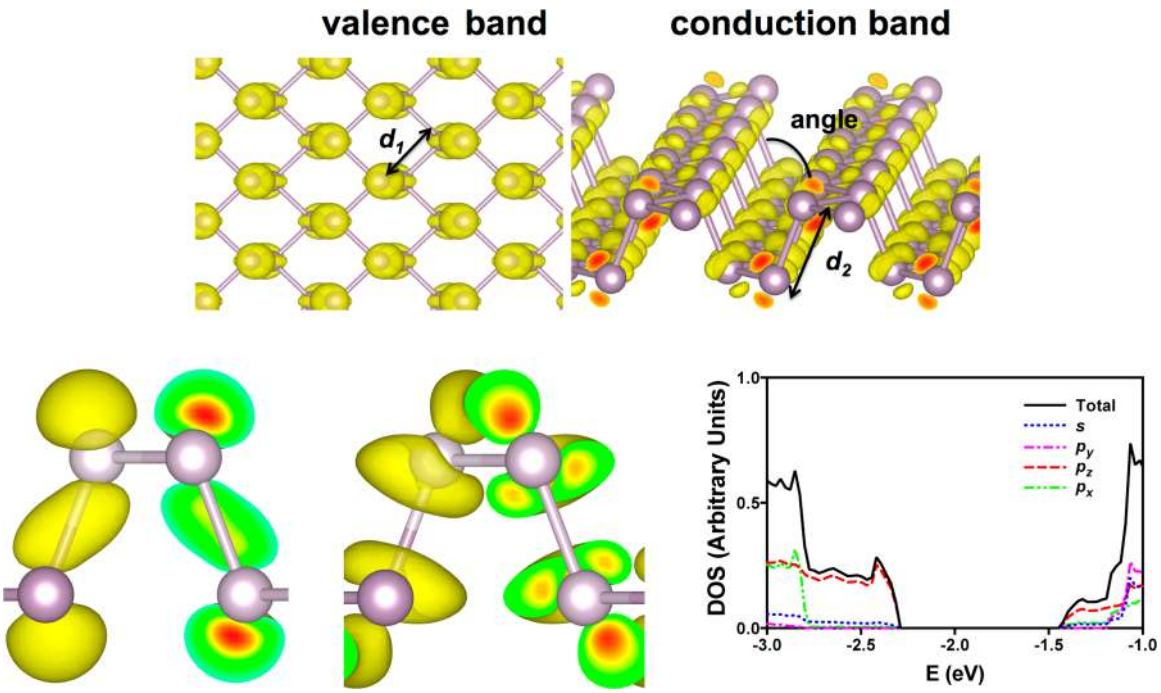

Figure 1. Atomic structure of phosphorene and partial electronic density of valence band edge (top left) and conduction band edge (top right) states (isosurface is set to 0.01 e/a_0^3). Bottom-left figure shows side view of VBM state; bottom-middle shows the side view of CBM state (isosurface set to 0.003 e/a_0^3); and bottom-right shows the total and partial DOSs.

Table 1. Structural Parameters, Bond Lengths and Angle, and Bandgap at Γ Point of Phosphorene

	a (Å)	b (Å)	d_1 (Å)	d_2 (Å)	angle (deg)	gap {Γ(eV)}
PBE	3.30	4.58	2.22	2.25	103.8	0.90
HSE06	3.28	4.54	2.20	2.23	104.0	1.55
						0.90 (PBE)
ref 12	3.35 (PBE)	4.62 (PBE)	N/A	N/A	N/A	1.1 (HSE)

and electronic structures optimized using the Perdew–Burke–Ernzerhof (PBE) functional.[26] Our results for the bulk were verified using the PBEsol functional[27] and the HSE06 hybrid functional.[28] The van der Waals stacking in bulk phosphorus was treated using the DFT-D2 method of Grimme.[29] Kohn–Sham orbitals are expanded in a plane wave basis set with a cutoff energy of 400 eV. All systems are relaxed until all forces are less than 0.01 eV/Å. A Monkhorst–Pack mesh of 8 × 8 × 1 was used for single layer phosphorene, whereas for nanoribbons the k-point mesh is 7 × 1 × 1. For these k-point meshes, the error is less than 1 meV per atom. For the calculation of band structures for the phosphorene sheet, we sample the following points of high symmetry: Γ, Y, and X, whereas for the ribbon we simply sample 20 points along the vector in reciprocal space that corresponds to the ribbon direction in real space. The vacuum region is set to 20 Å perpendicular to the sheet, with an additional 20 Å vacuum separating the nanoribbons.

Lattice parameter information for the bulk black phosphorus, calculated for PBE, PBESol, and HSE06 functionals, are given in the Supporting Information. From the analysis of the effects of van der Waals interactions (see Supporting Information), we clarify that for bulk phosphorus it is not necessary to modify the proportion of default exchange in order to obtain good agreement with experiment. For single-layer materials, for example, phosphorene, van der Waals corrections are not relevant and so were not included. Our results need only use the HSE06 functional for an accurate description of the electronic states of the monolayer. We also note that PBESol does not provide an accurate treatment of the crystal structure.

The calculated lattice parameters and bandgap at the Γ point of a single layer phosphorene (Figure 1) are listed in Table 1. In the absence of experimental information, we can only compare results with other simulations. As expected, van der Waals corrections are insignificant for phosphorene with equilibrium bond lengths and band gaps nearly the same. The bandgap from PBE calculations is in line with ref 12, ~0.9 eV; however, the bandgap from our hybrid functional is much higher at 1.55 eV. This difference is due to two factors: the model structure in ref 12 is from a nonhybrid PBE calculation, and their hybrid functional uses a reduced exchange contribution from the default value for the HSE06 functional. Furthermore, we note that the HSE06 functional accurately describes the bulk properties of many materials;[30] however, we caution that for nanostructures and surfaces hybrid functionals are not particularly accurate as they neglect the physically important enhancement of the self-interaction energy at the surface.[31,32] This problem results in an enhancement of exciton binding energies that is not captured by density functional approaches. The influence of model structure was subsequently investigated with the hybrid functional calculation, based on the PBE structure, yielding a bandgap of 1.30 eV.

In comparison with the literature on GW calculations of phosphorene with bandgaps reported of 1.6 and 2.0 eV.[18,33] our results are somewhat lower in magnitude. The underestimation

dx.doi.org/10.1021/nl501658d | Nano Lett. XXXX, XXX, XXX–XXX

reported by DFT is due to the improper treatment of the Coulomb repulsion. However, direct analysis of the band structure indicates that the primary difference between GW and DFT calculations is simply the position of the valence and conduction band;[33] effective masses would be similar. Our DFT calculations qualitatively capture the essential features of the band structure. With the observation that there is an increase in exciton binding energies for graphene nanoribbons,[32] we expect that the optical quantum size effect for very narrow ribbons will be less than predicted in our DFT calculations.

The energy of exfoliation of a single sheet of phosphorene was calculated using the PBE+vdW formalism. This exfoliation energy was found to be 0.339 Jm^{-2}, comparable in magnitude to that of graphene of 0.344 Jm^{-2}.[34]

The spatial distribution of the conduction and valence states of phosphorene were plotted, see Figure 1. From inspection, the valence band is mostly localized toward the exterior of the sheet, whereas the conduction band is more strongly weighted toward the interior of the sheet, that is, in between the two surfaces of the sheet. This behavior reflects the nature of the DOS, wherein both the valence band maximum (VBM) and conduction band minimum (CBM) have strong contributions from the p_z orbitals; the valence band edge is bonding-like when viewed from the projection into the sheet along the zigzag direction, and the conduction band edge antibonding-like, see Figure 1.

The band structure of phosphorene is calculated with the PBE and the HSE06 functionals, obtained using the relevant (PBE, HSE06) crystal structure. The findings are presented in Figure 2. The differences between the band structures are

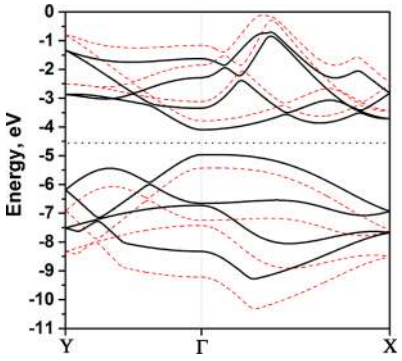

Figure 2. Calculated band structures of phosphorene, PBE structure with PBE functional (black solid line), HSE06 structure with HSE06 functional (red dash line). The zero of the *y*-axis is the reference level of the electrostatic potential in the middle of the vacuum region. The band structures of the two calculations were aligned using the electrostatic potential in the middle of the vacuum region.[35]

mostly due to a rigid shift upward in energy of the conduction band states and downward in energy of the valence band states. Importantly, there are no major qualitative differences in the dispersion of states across the special *k*-points.

With due consideration of the structure of phosphorene, there are three evident orientations to form nanoribbons: the armchair ribbon (a-PNR) along [100], the zigzag ribbon (z-PNR) along [010], and a diagonal ribbon (d-PNR) along [110] (which is at an angle of 35.7° to the armchair direction), see Figure 3. The formation of each nanoribbon results in the breaking of one P−P bond per edge phosphorus atom. In realistic nanostructures, these edge atoms are highly reactive

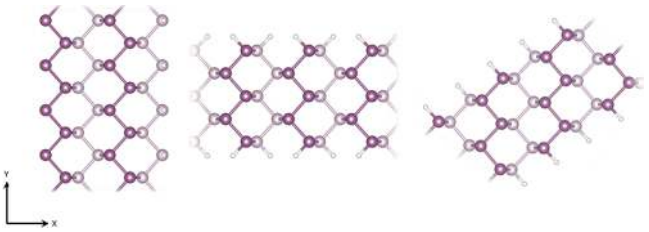

Figure 3. From left to right, z-PNR, a-PNR, and d-PNR. Axis definitions are the same as those shown in Table S1 (Supporting Information).

and will bond with impurities, especially hydrogen. Therefore, in our models the edges of the ribbon are passivated with hydrogen. In order to check for possible Peierls distortion effects that may modify the electronic structure by structural distortion,[36] we modeled several different lengths of nanoribbon, specifically ribbons of length one, two, and four unit cells. No such distortions were observed. The zero temperature edge formation energy per unit length (E_{edge}) was calculated using

$$E_{edge} = \frac{1}{2L}\left(E^{ribbon} - N_P E^{bulk} - \frac{N_H}{2}E_{H_2}\right)$$

where L is the length of the nanoribbon, E^{ribbon} is the total energy of the nanoribbon, N_P is the number of phosphorus atoms in the nanoribbon, E^{bulk} is the energy of phosphorene per atom, N_H is the number of hydrogen atoms, and E_{H_2} is the energy of a H_2 molecule. Our results are shown in Table 2.

Thermodynamically these cuts are slightly exothermic for the zigzag ribbons, which are stable with respect to depassivation. However, for both the armchair and diagonal nanoribbons the formation edges are slightly endothermic. The order of stability for these nanoribbons is z-PNR > d-PNR > a-PNR. For all the systems, the narrower the ribbon, the harder it is to form. We emphasize that these formation energies refer to zero-temperature; we would expect elevated temperatures to favor hydrogen release from the edges due to the entropic factor in the Gibbs free energy.

The magnitude of the bandgap in each type of the nanoribbon increases as the ribbon's width is reduced, see Figure 4. This effect is similar to that observed when forming graphene nanoribbons[37] and can be attributed to the quantum confinement of electrons.[38]

We see that the effect of quantum confinement when cutting perpendicular to the armchair direction to form z-PNRs is considerably greater than when cutting perpendicular to the zigzag direction to form a-PNR. For example, 13.5 Å wide z-PNR has a bandgap of 1.83 eV, while 13.2 Å wide a-PNR has a bandgap of only 1.01 eV. This finding is in line with the fact that the band edge states in phosphorene propagate primarily along the armchair direction. Furthermore, cutting phosphorene to form d-PNR also confines wave functions propagating in the armchair direction, although for a given width of ribbon the length scale of confinement is greater than when forming a-PNR and therefore the confinement effect is reduced. This change in bandgap originates from both an increase in energy of the conduction band edge, and a reduction in energy of the valence band edge. The bandgaps of the a-PNR structures and d-PNR structures are all direct, $\Gamma \rightarrow \Gamma$; however, for the z-PNR structures the lowest energy bandgap (by ~0.005 eV) is indirect, $0.0625 \rightarrow \Gamma$.

dx.doi.org/10.1021/nl501658d | *Nano Lett.* XXXX, XXX, XXX−XXX

Table 2. Number of P−P Rings, Defined as the 6-Atom Unit Cell As Illustrated by the Plane View in Figure 3, Nanoribbon Width, and Formation Energy of Ribbon Edges, for All Three Types of Nanoribbons

z-PNR			a-PNR			d-PNR		
width (rings*)	width (Å)	E_{edge} (meV)	width (rings)	width (Å)	E_{edge} (meV)	width (rings)	width (Å)	E_{edge} (meV)
11	27.2	−54	9	29.8	+55	9	26.3	+2
10	25.0	−54	8	26.5	+52	8	23.5	+2
7	18.0	−51	7	23.2	+55	7	20.7	+2
6	15.8	−49	6	19.9	+53	6	17.8	+3
5	13.5	−46	5	16.5	+55	5	15.0	+4
4	11.1	−45	4	13.2	+58	4	12.2	+6
3	8.8	−43	3	9.9	+59	3	9.3	+7
2	6.7	−32	2	6.6	+62	2	6.5	+10

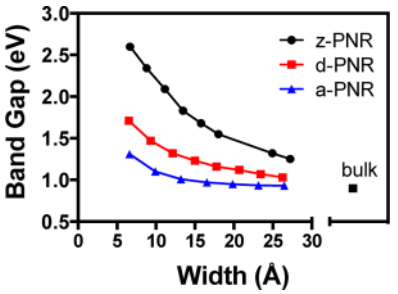

Figure 4. Variation of bandgap with respect to nanoribbon width for z-PNR, a-PNR, and d-PNR. The bulk value is also plotted.

For each type of PNRs, the bandgap was also calculated from the HSE06 functional to further verify the accuracy of the semilocal PBE functional. We found that the HSE06 bandgap was always higher than the PBE prediction. The difference of the band gaps between HSE06 and PBE calculations reduces gradually as the ribbon-width increases, varying from +0.81 eV (6.7 Å wide z-PNR), +0.68 (6.6 Å z-PNR), and +0.82 (6.5 Å d-PNR) to +0.68 eV (bulk).

The effective mass of electrons at the conduction band minimum (m_e^*) and of holes at the valence band maximum (m_h^*) were calculated using

$$m^* = \hbar^2\left(\frac{\partial^2 E}{\partial k^2}\right)^{-1}$$

where E and k correspond to energy and the reciprocal lattice vector along the nanoribbon. These nanoribbon effective masses were compared to those of the phosphorene sheet, specifically along the equivalent directions as the nanoribbons. The error in the PBE functional effective masses was determined by comparison to effective masses calculated with the HSE06 functional for the case of phosphorene. The PBE functional underestimates by 20.4% along the armchair direction and overestimates the effective mass by 10.8% along the zigzag direction. The effective masses determined by the PBE functional are sufficiently close to those by the HSE06 functional and allow us to be confident in the trends they predict.

A simplistic model, assuming velocity is randomized after each scattering event, gives the charge carrier mobility μ as

$$\mu = \frac{q}{m^*}\tau$$

where τ is the scattering time, q is the charge, and m^* is the effective mass. Changes in effective mass can influence charge carrier transport properties. Further, if there is no change in the time scale for quasiparticle scattering, then mobility is inversely proportional to the effective mass. However, especially for large strains, the scattering time may be altered which will then influence the mobilities. Detailed investigation of this effect is beyond the scope of this paper. Preliminary calculations on the phonon density of states show little difference for the unstretched and (+7%) stretched a-PNR structures, Supporting Information Figure S4. This would imply that, absent additional electron−phonon effects, the scattering time for unstrained and strained nanoribbons would be similar. Also, in the following discussion we note there are no significant changes in structural parameters associated with the abrupt changes in effective masses. Significant changes in effective masses would be expected to alter charge carrier transport properties.

Effective masses for the majority of the a-PNRs are very similar to those along the analogous armchair direction in phosphorene, where $m_h^* = 0.15m_0$ and $m_e^* = 0.16m_0$ (m_0 is the mass of the electron). For example, in 26.5 Å wide a-PNR, $m_h^* = 0.15m_0$ and $m_e^* = 0.17m_0$. However, for very narrow a-PNR structures the electron transport at the CBE is quenched, for example, in 9.9 Å wide a-PNR $m_e^* = 1.40m_0$. Nanostructuring along this direction can potentially affect n-type conductivity.

Similarly, effective masses along the wider z-PNR structures are comparable to those along the analogous zigzag direction in bulk phosphorene, where $m_h^* = 1.54m_0$ and $m_e^* = 1.23m_0$. For example, in 27.2 Å wide z-PNR, $m_h^* = 1.55m_0$ and $m_e^* = 1.31m_0$. However, for very narrow z-PNR structures, the hole transport at the VBM is quenched, for example, in 8.8 Å wide z-PNR $m_h^* = 5.00m_0$. Nanostructuring along this direction can potentially affect p-type conductivity.

For the d-PNR structures, the effective masses of both hole and electrons are comparable. For 26.3 Å wide nanoribbons $m_h^* = 1.03m_0$ and $m_e^* = 0.60m_0$. Unlike the other nanoribbons, nanostructuring does not strongly modify these values, for example, for the narrowest d-PNR, $m_h^* = 0.73m_0$ and $m_e^* = 0.68m_0$. Nanostructuring along this direction does not especially improve transport of either type of charge carrier.

In general, in terms of truncating the crystal lattice and maximizing charge transport (assuming there is no change in the time scale for electron scattering), a-PNR nanoribbons are best, as effective masses along this direction are smaller than in other directions, which is no doubt due to the strong p_z contributions to the VBE and the CBE. The natural direction for charge transport is through these states, and the greatest overlap between these orbitals is from one side of the sheet to the other, that is, from top to bottom, which corresponds to the armchair direction; therefore a-PNR nanoribbons, which maintain the structure along the armchair direction, are best. The effective masses for a-PNRs compare favorably with those

dx.doi.org/10.1021/nl501658d | Nano Lett. XXXX, XXX, XXX−XXX

reported for graphene nanoribbons, which are of the order 0.06 to 0.21 m_0.[39,40]

Properties of nanoribbons may be easily modified through the application of uniaxial strain. In order to investigate their response to straining, we applied uniaxial strain along the infinite direction of each type of PNR, calculated the in-plane stiffness, and investigated the effects of straining on bandgap and effective mass in order to provide insight into the charge transport properties. We present results for the widest nanoribbons only but similar trends hold for other nanoribbon widths. We investigate strains up to a magnitude of ±10%, which is considerably less than the theoretical ultimate strain of phosphorene and thus is physically realizable.[41,42] We have calculated the in-plane stiffness, C, of the different nanoribbon structures. Tabulated values are given in the Supporting Information. The a-PNR structures are easiest to compress, the d-PNR structures are the easiest to extend. These results are in line with recent studies on bulk phosphorene that found that the surface tension of phosphorene under a given strain is considerably lower in the armchair direction than in the zigzag direction.[43] The values are a factor of 10 less than that reported for graphene structures[44] and are due to the puckered structure of phosphorene where compression or extension mainly leads to P−P−P bond angle change.

We calculated the bandgap and effective masses of a-PNR structures at strains between $\varepsilon = -10\%$ and +10%, see Figure 5.

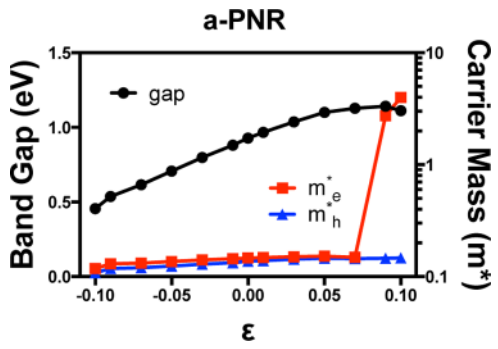

Figure 5. Variation of bandgap (shown in left axis); hole and electronic effective masses (shown in right axis) with respect to strain (ε) for the a-PNR.

Under no strain, we found that the effective mass of the hole is slightly lower than that of the electron. The effect on the electronic structure of stretching a-PNR between $\varepsilon = -10\%$ and +8% is dominated by the stabilization of the VBM, which has a maxima at the Γ-point and consists of p_z orbitals that are antibonding (out-of-phase) in the armchair direction, see Figure 6. As the a-PNR is stretched and the antibonding p_z orbitals are separated, the VBM is stabilized, lowering in energy. This results in the bandgap increasing from 0.46 eV at $\varepsilon = -10\%$ to 1.16 eV at $\varepsilon = +8\%$. The effective mass of this band, m_h^*, also increases as the structure is stretched, rising from $0.11m_0$ at $\varepsilon = -10\%$ to $0.15m_0$ at $\varepsilon = +10\%$. This can be readily explained as a reduction in overlap between p_z orbitals as a-PNR is stretched. It should also be noted that as the a-PNR is compressed, a competing valence band with its maxima at [0.5, 0, 0] rises in energy. At strains of $\varepsilon \leftarrow 10\%$, there is a dramatic change in the VBM character as the bandgap of a-PNR becomes indirect from X → Γ.

Meanwhile, the CBM of unstrained a-PNR consists of p_z orbitals that are nonbonding in the armchair direction. The

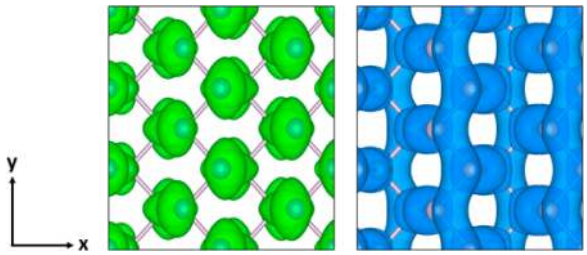

Figure 6. VBM (left) is nonbonding in the zigzag direction, implying that its upon extension the energy does not change. The CBM (right) is bonding in the zigzag direction, meaning that it is destabilized upon extension. Armchair direction is along X, zigzag direction is along Y. Isosurfaces are 0.001 e/a_0^3.

CBM is therefore energetically unchanged as a-PNR is strained between $\varepsilon = -10\%$ and +8%, and trends in the bandgap of a-PNR are dominated by the VBM energy. However, as a-PNR is stretched a higher energy conduction band made up of antibonding p_y orbitals reduces in energy and becomes stabilized relative to the CBM. At strains of $\varepsilon > +8\%$, this band becomes the CBM and continues to fall in energy as a-PNR is stretched, causing the bandgap to plateau and begin to fall. This new CBM is also extremely flat and nondispersive near the conduction band minimum, see Supporting Information Figure S1, leading to a dramatic increase in m_e^* at strains of $\varepsilon > +8\%$, potentially leading to a quenching of charge transport in the conduction band as m_e^* rises to $\approx 4m_0$ while m_h^* is unaltered.

In summary, stretching a-PNR between $\varepsilon = -10\%$ and +8% leads to a steadily increasing hole and electron effective mass m_e^*/m_h^* ratio and bandgap due to orbital separation and the stabilization of the VBM respectively. At strains above 8%, a new CBM emerges and is stabilized as further strain is applied, reducing the bandgap but strongly increasing the electron effective mass. This exceptional increase in the ratio m_e^*/m_h^* means that this structure may readily be tuned for p-type applications (Figure 7).

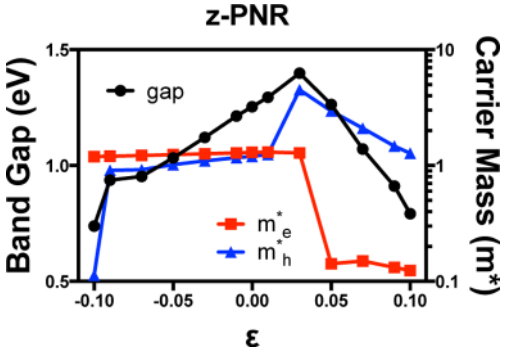

Figure 7. Variation of bandgap (shown in left axis); hole and electronic effective masses (shown in right axis) with respect to strain (ε) for the z-PNR.

For z-PNR structures, a different behavior is manifested. At zero strain, the effective mass of the hole is slightly less than that of the electron. The p_z orbitals making up the VBM, which is located at [0, 0.0625, 0], are nonbonding in the zigzag direction, so the stabilization of the VBM seen when stretching a-PNR is not seen in z-PNR. Instead, the increase in bandgap seen between −9% and +3% is attributable to the

dx.doi.org/10.1021/nl501658d | Nano Lett. XXXX, XXX, XXX−XXX

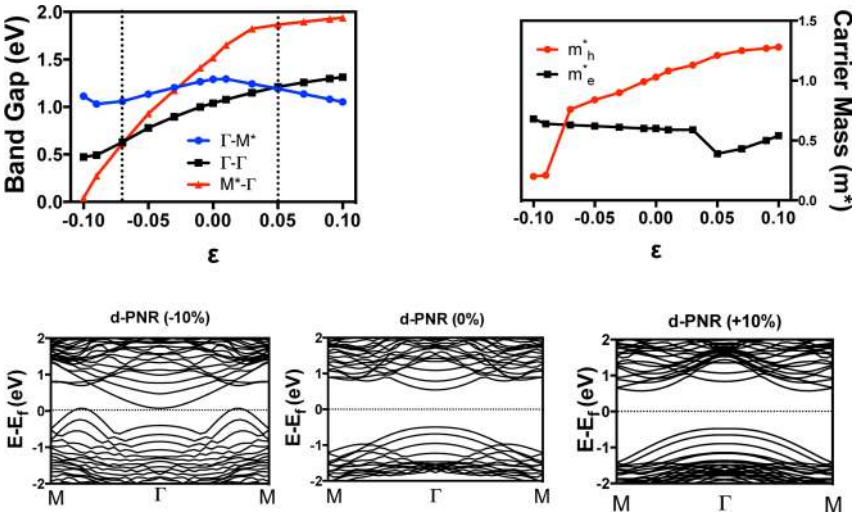

Figure 8. Variation of bandgap (top left) and hole and electronic effective masses (top right) with respect to strain (ε) for the d-PNR, both direct transition ($\Gamma \rightarrow \Gamma$ black line with squares), and two indirect transitions ($\Gamma \rightarrow$ M*, blue line with circles, M* $\rightarrow \Gamma$, red line with triangles). The dashed lines indicate where the transition from a direct to an indirect bandgap occurs. Bottom figures are representative band structures for strains of −10, 0, and +10%, respectively.

destabilization of the CBM. As can be seen in Figure 6, the CBM consists of p_z orbitals that are bonding in the zigzag direction. Therefore, stretching z-PNR destabilizes the CBM and increases the band gap. However, as z-PNR is stretched past ε = +4%, a new CBM emerges that consists of p_z orbitals arranged in an antibonding manner along the zigzag direction. This band has a greater dispersion along the nanoribbon direction than the original CBM, see Supporting Information Figure S3. Extension of z-PNR stabilizes these orbitals and causes the bandgap to fall. Furthermore, m_e^* falls by an order of magnitude as strain exceeds ε = +4%. Meanwhile, a new VBM emerges at the Γ point when ε > +3%, making the bandgap direct ($\Gamma \rightarrow \Gamma$). We note that the direct bandgap is typically only a hundredth of an electronvolt higher than the indirect gap for cases where indirect gaps are lowest in energy. This VBM is nondispersive, see Supporting Information Figure S2, resulting in a significant jump in m_h^* when strain exceeds ε = +3% with the effective hole mass reaching values of 4.5 m_0. The sharp drop in m_h^* and bandgap observed when ε = −10% can be attributed to a rising VBM made up of antibonding p_x orbitals.

To summarize, compressing z-PNR nanostructures shows a significant effect on hole effective mass, strongly influencing hole transport. Conversely, placing z-PNR nanostructures under tensile strain significantly reduces the electron effective mass, while strongly increasing the hole effective mass, potentially quenching hole transport. The ratio of m_h^*/m_e^* is liable to demonstrate a giant increase after a tensile strain of 4%; this has significant implications for potential switching devices. This structure may be tuned for n-type applications.

In contrast to the a-PNR and z-PNR structures, the behavior of the bandgap with respect to external strain for the d-PNR structures is rather complicated, see Figure 8. The direct bandgap (which involves a $\Gamma \rightarrow \Gamma$ transition) increases linearly with increasing tensile strain and conversely decreases with increasing compressive strain. This behavior is driven by the behavior of the valence and conduction bands. The conduction band rises in energy with tension and decreases in energy upon compression. The constituent p_z orbitals are arranged in an overall bonding manner along the infinite ribbon direction. The valence band is mostly composed of p_z orbitals that are mostly antibonding in character, which extend along the nanoribbon direction. Therefore, upon extension the valence band slightly lowers in energy. As d-PNR is stretched between ε = +0% and +10%, the energy of the conduction band at point M* (0.276, 0.276, 0) falls, reducing the $\Gamma \rightarrow$ M* gap. When ε = +5%, the CBM moves to M* and the bandgap of d-PNR becomes indirect ($\Gamma \rightarrow$ M*). The $\Gamma \rightarrow$M* gap continues to decrease with tensile strain, falling to 1.05 eV at ε = +10%. While the energy of the valence band at the Γ-point only slightly alters, the energy of the valence band at M* rises as d-PNR is compressed. This behavior is related to the buckled nature of the material and the bonding nature of the p_z orbitals at that point. As the nanoribbon is compressed, the distance between the top and bottom layers increases, which destabilizes the bonding orbitals leading to a rise in their energy. Consequently this manifests at the valence band edge when ε = −7%, the VBM moves from Γ to M*, and the bandgap of d-PNR becomes indirect (M*− Γ). As d-PNR is further compressed, the bandgap falls and eventually begins to exhibit metallic character at ε = −10%.

It follows from the above discussion that there are critical strain values where the Γ- and M*-point energies are equal. For the valence band, the critical strain value is around −7%, whereas for the conduction band it is around +5%. This behavior would have potential applications for valleytronic devices, which make use of the fact that quasiparticles with the same energy, but residing in different parts of the reciprocal space, have different momenta and thus are less susceptible to phonon scattering.[45]

The effective masses of the electron and hole in the d-PNR were also calculated, as shown in Figure 8. Under no external strain, the effective mass of the electron is significantly less than that of the hole, which is in contrast to the other two nanoribbon structures studied. When under compressive strain, the effective mass of the electron slightly increases; however, there is a significant decrease in the effective mass of the hole, especially when the bandgap undergoes a transition from direct to indirect at −9%. Initially m_h^* = 1.03m_0, but falls to 0.20m_0 when compressive strain is −9%. When the nanoribbon is under a tensile strain, hole masses slowly increase to 1.28m_0 at

dx.doi.org/10.1021/nl501658d | Nano Lett. XXXX, XXX, XXX−XXX

strain +10%, while m_e^* slowly decreases to $0.39m_0$ at +3% strain before increasing again to $0.54m_0$ for a strain of +10%. This behavior is due to the onset of the direct−indirect transition. To summarize, compressing d-PNR improves hole effective masses, and for large compressive and tensile strains the direct to indirect transition strongly reduces the gap, which also coincides with a strong decrease in the hole effective mass. Upon tension, the electron effective mass remains smaller than the hole mass, even when the direct−indirect transition occurs at a tension of +5%.

From the above analysis of the behavior of the effective masses, it is clear that putting both a-PNR and z-PNR structures under tensile strain is optimal for tuning phosphorene nanoribbons for p-type (hole-dominated transport for the a-PNR) and n-type (electron dominated transport for the z-PNR) devices. However, if maximized charge transport of both types of carrier is desired, then nanoribbons should be placed under compressive strain. The d-PNR structures demonstrate an interesting direct to indirect transition for both compression and extension, which modify the optical properties, but based on analysis of the band structure, we determine that at critical strains it is possible to achieve degenerate energy valleys at different *k*-points. Nanostructuring of the material in this direction would be of interest for valleytronic applications. Overall, for effective masses the a-PNR structures are best as those possess the lowest masses.

It is interesting to compare the effects of straining all three nanoribbons to that of straining two-dimensional phosphorene.[43] While the effects of uniaxial strain on phosphorene manifest as changes in the electronic structure in all directions of the 2D reciprocal space, the pseudo one-dimensional nature of nanoribbons means that the Brillouin zone can only be sampled in one direction. For example, the direct to indirect bandgap transition observed when stretching phosphorene is not observed when stretching a-PNR. This is because a new CBM emerges between Γ and Y in the reciprocal space when stretching phosphorene, which cannot be sampled in the one-dimensional Brillouin zone of the a-PNR structure.

In summary, we have performed density functional theory simulations on a realistic model for passivated phosphorene nanoribbons, a one-dimensional nanostructure that demonstrates the anisotropy of the phosphorene lattice. We found that gradient-corrected functionals are sufficient to calculate effective masses. We show that in order to describe correctly the electronic properties of bulk black phosphorus, it is essential to include van der Waals effects.

Three types of nanoribbon were constructed and modeled, all of which involved the breaking of one P−P bond per edge phosphorus atom, the armchair, diagonal, and zigzag. All three types of nanoribbon display quantum size effects that modify the position of the valence and conduction band edges with decreasing width, allowing tuning of the bandgap. In particular, the z-PNR structures show strong quantum size effects with a large change in bandgap over the ribbon widths. Nanostructuring to very narrow widths does change the effective mass of carriers. Nanostructuring of a-PNR increases the electron effective mass by an order of magnitude. Nanostructuring of z-PNR increases the hole effective mass by a factor of 3. Carrier effective mass in d-PNR structures are insensitive to nanostructuring. Such phenomenon can be effectively utilized for electron−hole separation, for example, in photocatalysis.

The response of the nanoribbons to strain was also determined. Strain was found to change the relative energy and nature of electronic states within the nanoribbons, leading to changes in the bandgap and effective masses. The effect of strain on the bandgap can be understood by looking at the bonding character of the band edges along the direction of straining. Meanwhile, when nanoribbons are stretched or compressed passed critical strains, competing bands rise or fall in energy and assume band edge positions, leading to dramatic shifts in m_h^* and m_e^*. Remarkably, for a-PNR structures upon surpassing the critical strain of +9% the effective mass of the electron is increased by a factor of 30 while leaving the hole effective mass unchanged. Similarly, for z-PNR, straining to +4% results in a giant increase in m_h^*/m_e^*, a behavior that has great potential for switching devices.

Furthermore, straining d-PNR can lead to two direct to indirect bandgap transitions as the valence band is stabilized (under compression) and the conduction band is destabilized (under extension) at a special *k*-point M*, which is widely separated from the Γ-point. There is the possibility that d-PNR structures may be engineered upon straining, so that two energetically degenerate valleys with electrons of widely different momentum are able to coexist at the same energy. These materials are thus of interest for valleytronic applications.

Phosphorene is a material that possesses great potential for electronic and optical devices. We demonstrate that electronic properties can be tuned by fabrication of nanoribbons. We show in particular that strain can improve charge transport properties with tension potentially improving the electron transport of a-PNR structures and hole transport properties of z-PNR structures. Furthermore, the optical properties of d-PNR structures can be tuned and further experimental investigation of these structures would be of great interest.

■ ASSOCIATED CONTENT

Ⓢ Supporting Information

Comparison of structural parameters and electronic structure for black phosphorus obtained using PBE, PBESol, HSE06, PBE+Grimme, and HSE06+Grimme functionals. Effective masses and bandgaps of phosphorene nanoribbons for strain values are tabulated. Stiffness constants of three types of PNR are also tabulated. Analysis of band behavior when a-PNR and z-PNR structures are strained. This material is available free of charge via the Internet at http://pubs.acs.org.

■ AUTHOR INFORMATION

Corresponding Author

*E-mail: z.x.guo@ucl.ac.uk.

Notes

The authors declare no competing financial interest.

■ ACKNOWLEDGMENTS

We acknowledge our membership of the UK's HPC Materials Chemistry Consortium, which is funded by EPSRC (EP/L000202). The authors would also acknowledge the use of the UCL Legion High Performance Computing Facility (Legion@UCL), the HECToR High Performance Computing Facility, and associated support services in the completion of this work. EU funding by the 4G-PHOTOCAT consortium (Project Number 309636). X.H.Y. would like to thanks the Chinese Scholarship Counsel (CSC) and British Department for Business, Innovation and Skills (BIS) and UCL for financial

support. Mr. David Mora-Fonz is acknowledged for useful discussions.

REFERENCES

(1) Yu, W. J.; Li, Z.; Zhou, H.; Chen, Y.; Huang, Y.; Duan, X. *Nat. Mater.* **2013**, *12*, 246−252.
(2) Lee, D. H.; Gupta, J. A. *Science* **2010**, *330*, 1807−1810.
(3) Shevlin, S. A.; Currioni, A.; Andreoni, W. *Phys. Rev. Lett.* **2005**, *94*, 146401.
(4) Novoselov, K. S.; Fal'ko, V. I.; Columbo, L.; Gellert, P. R.; Schwab, M. G.; Him, K. *Nature* **2012**, *490*, 192−200.
(5) Wang, H.; Wang, Q.; Cheng, Y.; Li, K.; Yao, Y.; Zhang, Q.; Dong, C.; Wang, P.; Schwingenschlögl, U.; Yang, W.; Zhang, X. X. *Nano Lett.* **2012**, *12*, 141−144.
(6) Cai, J.; Riffieux, P.; Jafar, R.; Bieri, M.; Braun, T.; Blankenburg, S.; Muoth, M.; Seitsonen, A. P.; Saleh, M.; Feng, X.; Müllen, K.; Fasel, R. *Nature* **2010**, *466*, 470−473.
(7) Mohanty, N.; Moore, D.; Xu, Z.; Sreepasad, T. S.; Nagaraja, A.; Rodriguez, A. A.; Berry, V. *Nat. Commun.* **2012**, *3*, 844.
(8) Barone, V.; Hod, O.; Scuseria, G. *Nano Lett.* **2006**, *6*, 2748−2754.
(9) Wang, X.; Ouyang, Y.; Li, X.; Wang, H.; Guo, J.; Dai, H. *Phys. Rev. Lett.* **2008**, *100*, 206803.
(10) Lee, J.-K.; Yamazaki, S.; Yun, H.; Park, J.; Kennedy, G. P.; Kim, G.-T.; Pietzsch, O.; Wisendanger, R.; Lee, S. W.; Hong, S.; Dettlaff-Weglikowska, U.; Roth, S. *Nano Lett.* **2013**, *13*, 3494−3500.
(11) Zhao, F.; Nguyen, T. T.; Golsharifi, M.; Amakubo, S.; Loh, K. P.; Jackman, R. B. *J. Appl. Phys.* **2013**, *114*, 053709.
(12) Liu, H.; Neal, A. T.; Zhu, Z.; Tománek, D.; Peide, D. Ye *ACS Nano* **2014**, DOI: 10.1021/nn501226z.
(13) Li, L.; Yu, Y.; Ye, G. J.; Ge, Q.; Ou, X.; Wu, H.; Feng, D.; Chen, X. H.; Zhang, Y. *Nat. Nanotechnol.* **2014**, DOI: 10.1038/nnano.2014.35.
(14) Reich, E. S. *Nature* **2014**, *506*, 19.
(15) Xia, F.; Wang, H.; Jia, Y. arXiv:1402.0270 2014.
(16) Castellanos-Gomez, A.; Vicarelli, L.; Prada, E.; Island, J. O.;Narasimha-Acharya, K. L.; Blanter, S. I.; Groenendijk, D. J.; Buscema, M.; Steele, G. A.; Alvarez, J. V., Zandbergen, H. W.; Palacios, J. J.; van der Santt, H. S. J. arXiv: 1403.0499 2014.
(17) Zhu, Z.; Tománek, D. *Phys. Rev. Lett.* **2014**, *112*, 176802.
(18) Tran, V.; Soklasi, R.; Liang, Y.; Yang, L. arXiv:1402.4192 2014.
(19) Baringhaus, J.; Ruan, M.; Edler, F.; Tejeda, A.; Sicot, M.; Taleblbrahimi, A.; Li, A.; Jiang, Z.; Conrad, E. H.; Berger, C.; Tegenkamp, C.; de Heer, W. A. *Nature* **2014**, DOI: 10.1038/nature12952.
(20) Tran, V.; Yang, L. arXiv:1404.2247 2014.
(21) Peng, X.; Wei, Q.; Copple, A. arXiv:1404.5995 2014.
(22) Guo, H.; Lu, N.; Dai, J.; Wu, X.; Zeng, X. C. arXiv:1403.6209 2014.
(23) Fei, R.; Yang, L. arXiv:1403.1003 2014.
(24) Blöchl, P. E. *Phys. Rev. B* **1994**, *50*, 17953−17979.
(25) Kresse, G.; Hafner, J. *Phys. Rev. B* **1993**, *47*, 558−561.
(26) Perdew, J. P.; Burke, K.; Ernzerhof, M. *Phys. Rev. Lett.* **1996**, *77*, 3865−3868.
(27) Perdew, J. P.; Ruzsinszky, A.; Csonka, G. I.; Vydrov, O. A.; Scuseria, G. E.; Constantin, L. A.; Zhou, X.; Burke, K. *Phys. Rev. Lett.* **2008**, *100*, 136406.
(28) Heyd, J.; Cruseria, G. E.; Ernzerhof, M. *J. Chem. Phys.* **2003**, *118*, 8207−8215.
(29) Grimme, D. *J. Comput. Chem.* **2006**, *27*, 1787−1799.
(30) Krukau, A. V.; Vydrov, O. A.; Izmaylov, A. F.; Scuseria, G. E. *J. Chem. Phys.* **2006**, *125*, 224106.
(31) Yang, L.; Park, C.-H.; Son, Y.-W.; Cohen, M. L.; Louie, S. G. *Phys. Rev. Lett.* **2007**, *99*, 186801.
(32) Jain, M.; Chelikowsky, J. R.; Louie, S. G. *Phys. Rev. Lett.* **2011**, 216806.
(33) Rudenko, A. N.; Katsnelson, M. I., arXiv:1404.0618 2014.
(34) Faccio, R.; Denis, P. A.; Pardo, H.; Goyenola, C.; Mombrú, Á.W. *J. Phys.: Condens. Matter* **2009**, *21*, 285304.
(35) Walsh, A.; Catlow, C. R. A. *J. Mater. Chem.* **2010**, *20*, 10438−10444.
(36) Shevlin, S. A.; Fisher, A. J.; Hernandez, E. *Phys. Rev. B* **2001**, *63*, 195306.
(37) Son, J. W.; Cohen, M. L.; Louie, G. *Phys. Rev. Lett.* **2006**, *97*, 216803.
(38) Yoffe, A. D. *Adv. Phys.* **1993**, *42*, 173−262.
(39) Ruffiex, P.; Cai, J.; Plumb, N. C.; Pathey, L.; Prezzi, D.; Feretti, A.; Molinari, E.; Feng, X.; Müllen, K.; Pignedoli, C. A.; Fasel, R. *ACS Nano* **2012**, *6*, 6930−6935.
(40) Tayo, B. O. arXiv:1404.2499 2014.
(41) Wei Q.;Peng, X. arXiv:1403.7882 2014.
(42) Jiang, J.-W.; Park, H. S. arXiv:1404.0232 2014.
(43) Peng, X.; Copple, A.; Wei, Q. arXiv:4371 2014.
(44) Faccio, R.; Denis, P. A.; Pardo, H.; Goyenola, C.; Mombrú, Á.W. *J. Phys.: Condens. Matter* **2009**, *21*, 285304.
(45) Zeng, H.; Dai, J.; Yao, W.; Xiao, D.; Cui, X. *Nat. Nanotechnol.* **2012**, *7*, 490−493.